Acta Polytechnica CTU Proceedings **25**:17–20, 2019
doi:10.14311/APP.2019.25.0017

available online at http://ojs.cvut.cz/ojs/index.php/app

COMPRESSIVE PROPERTIES OF AUXETIC STRUCTURES WITH CONTROLLED STIFFNESS OF STRUT JOINTS

Tomáš Doktor*, Tomáš Fíla, Petr Koudelka, Daniel Kytýř, Ondřej Jiroušek

Czech Technical University in Prague, Faculty of Transportation Sciences, Konviktská 20, 110 00 Prague, Czech Republic

* corresponding author: doktor@fd.cvut.cz

Abstract. Presented paper deals with experimental study on compressive properties of auxetics with controlled stiffness of strut joints. The variable strut joints properties were simulated by adding extra amount of material in the struts' intersection regions. Four groups of inverted honeycomb structures were prepared by multi-jet 3D printing and tested in quasi-static compression. The structure collapsed gradually, however after the first collapse, failure in entire cross-section occurred due to the brittle nature of the base material. The behavior up to the first collapse was consistent among the specimens within each group, while differed slightly subsequently. With higher reinforcement in the joints, results showed increasing stress at the first collapse (ultimate compressive stress) while the strain at the first collapse remained unchanged. The auxetic behaviour became less significant with increasing joints' reinforcement.

Keywords: Auxetics, cellular materials, quasi-static testing, optimisation, additive manufacturing.

1. Introduction

It has been already shown that cellular solids are able to absorb tremendous amounts of deformation energy [1, 2] during impacts with the possibility to introduce strain-rate dependent characteristics into their deformation response [3]. However, certain applications, such as blast and flying debris protection systems, may require material with relatively high strength in addition to excellent deformation absorption capabilities. Such complex mechanical characteristics can be achieved without alteration of the existing lightweight alloys (such as aluminium based materials) used for the material's production when the microstructure is constructed in such a way to exhibit negative Poisson's ratio [4]. Mechanical characteristics of such auxetic lattices are given not only by overall geometrical arrangement of struts in the unit cell and their connectivity but also by deformation properties of the strut joints. There are two main mechanisms of the lattice behaviour during mechanical deformation. Based on the struts' connectivity the deformation is stretching dominated for lattices which comply with truss assumptions or bending dominated in lattices with incomplete connectivity [5]. Hence the deformation and energy absorption properties are highly influenced by the bending in the struts' connections. Influence of all these factors on effective mechanical properties in both elastic and plastic regime has to be thoroughly evaluated and taken into account in analytical and numerical optimisation. In this paper a parametric study on influence of the strut joint stiffness on the effective deformation response of various auxetic lattices is presented.

2. Materials and methods

2.1. Specimen design and manufacturing

Auxetic lattices exhibiting negative Poisson's ratio were designed in parametric modeller SolidWorks (Dassault Systémes Corp., France). Three-dimensional inverted honeycomb was selected which exhibits auxetic behaviour in all three dimensions. Design of the tested auxetic structure was based on our previous study [6], in which first preliminary results were presented. Only entirely auxetic structures were used in contrary to the planar auxetics. The porosity and ratio between cell size and strut cross-section (square shaped) was accommodated for a better stiffness and strength. At the top and bottom plane plate was added in to ensure a better force transfer between the loading grips and the specimens. Design parameters of the specimens are listed in table 1, geometry of the unit cell is depicted in Fig. 1.

Specimen height	[mm]	26
Specimen cross-section	[mm]	16.5×16.5
Number of unit cells	[–]	$3 \times 3 \times 3$
Strut cross-section	[mm]	0.75×0.75

Table 1. Design parameters - common parameters.

Different joint stiffness was achieved by differently sized spheres placed in the intersections of the struts. Three different radii were selected. Upper limit value of the spheres' radius (1.875 mm) was selected to avoid contact between neighboring spheres. The lower limit (0.938 mm) was selected with respect to a possible observation of the reinforcing effect, as smaller spheres

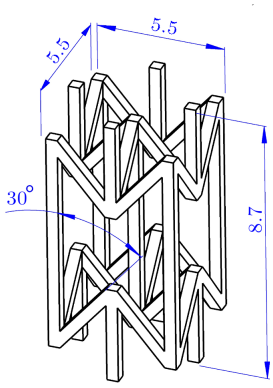

Figure 1. Geometry of the unit cell.

would be entirely hidden in the intersection of the prismatic struts. Parameters of the joints' reinforcement are listed in table 2.

Group	Sphere radius [mm]	Porosity [%]
0	-	78.8
1	0.75	76.9
2	0.9375	72.4
3	1.125	64.9

Table 2. Design parameters - joint reinforcement variations.

STL models which were used for the 3D printing of tested samples are depicted in figure 2. The specimens were manufactured by direct 3D printing from UV-curable acrylic material VisiJet EX200 (3D Systems, USA) using 3D printer Pro Jet HD3000 (3D Systems, USA) in high definition mode. Resolution in high definition mode was $387 \times 387 \times 300$ dpi.

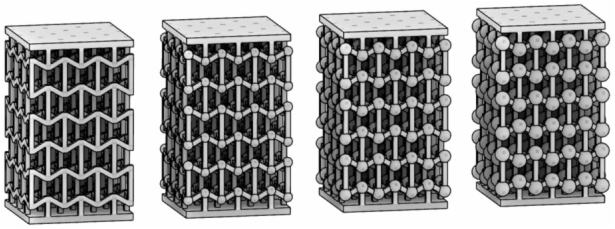

Figure 2. STL models for 3d printing.

2.2. Compression tests

For the compression experiments a custom loading device was used equipped with force transducer with loading capacity 2 kN (U9b, Hottinger Baldwin Messtechnik GmbH, Germany). The loading was provided by a stepper motor controlled by LinuxCNC software solution used with real-time GNU/Linux operating system [7]. The tests were displacement driven with loading rate $20\mu m \cdot s^{-1}$. Contactless displacement measurement was employed based on digital image correlation (DIC) [8, 9]. The loading scene was captured by a CCD camera (Manta G504B, Alied Vision Technologies GmbH, Germany) attached to a

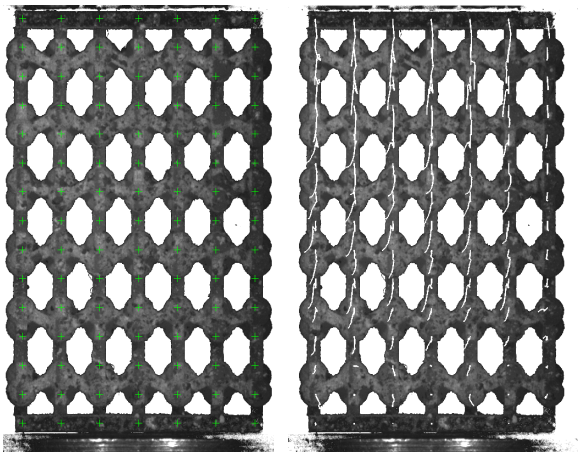

Figure 3. Loading scene with tracking features (left) and tracked displacement paths (right). Black background was inverted due to a better visibility.

bi-telecentric zoom lens (TZCR 072, OptoEngineering, Italy). The image data was captured with a custom software tool based on OpenCV library [10]. Zoom ratio $0.25\times$ was used for all compressive tests, which provided pixel-size 13.7 μm. A set of tracking features was selected in the first (undeformed) loading scene which were arranged into 7 columns and 15 rows to ensure placement of the features in solid material of the struts. The array of loading features is depicted in figure 3 (left). The loading rate together with the frame rate 2 fps ensured a sufficient number of points in the obtained loading curve. Figure 3 (right) shows displacement paths tracked by DIC in selected specimen from group 2.

2.3. Evaluation

The measured displacements and forces were used to calculate engineering strain ϵ_{eng} and stress σ_{eng} which were converted into true strain ϵ_{true} and true stress σ_{true} using formulae (1) and (2), respectively.

$$\epsilon_{true} = ln(1 + \epsilon_{eng}) \tag{1}$$

$$\sigma_{true} = \sigma_{eng} \cdot (1 + \epsilon_{eng}) \tag{2}$$

Based on measured strain in transversal and longitudinal direction, Poisson's ratio was calculated according to formula (3).

$$\mu = -\frac{\epsilon_x}{\epsilon_y} \tag{3}$$

To exclude values which correspond to both initial settlement and post-yield region after the first plastic collapse, the function of Poisson's ratio was limited only inside these limit values of strain. Moreover, to assess the influence of joints' stiffness on the mechanical behaviour, ultimate compressive stress of the tested structures was evaluated as well as strain corresponding to the first plastic collapse.

Group	σ_m [MPa]	ϵ_{y1} [1]	μ_{mean} [1]
0	0.876 ± 0.124	0.0383 ± 0.0032	-0.180 ± 0.040
1	0.887 ± 0.134	0.0348 ± 0.0029	-0.219 ± 0.058
2	0.942 ± 0.138	0.0346 ± 0.0030	-0.142 ± 0.030
3	1.168 ± 0.054	0.0352 ± 0.0027	-0.047 ± 0.065

TABLE 3. Average results in tested groups. Stress and strain at the first collapse. Average Poisson's number.

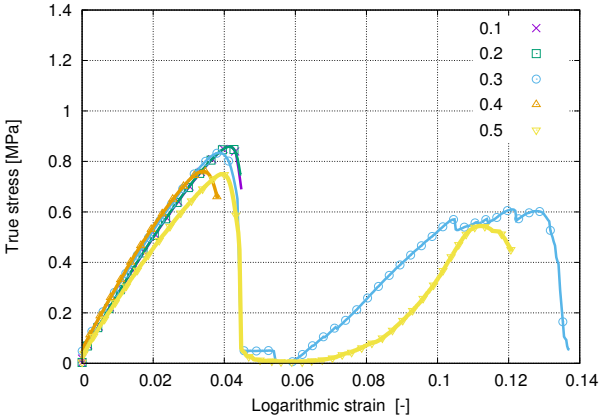

FIGURE 4. Stress-strain curves of specimens in group 0.

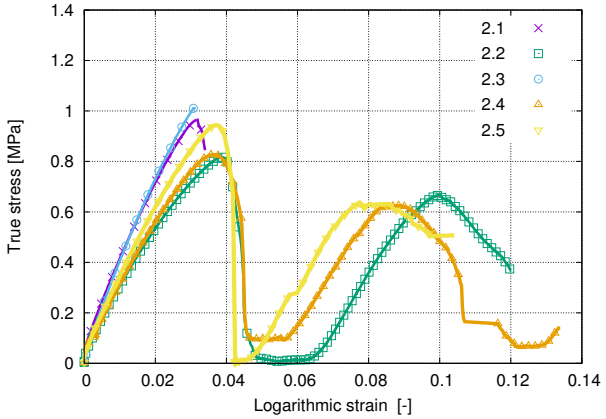

FIGURE 6. Stress-strain curves of specimens in group 2.

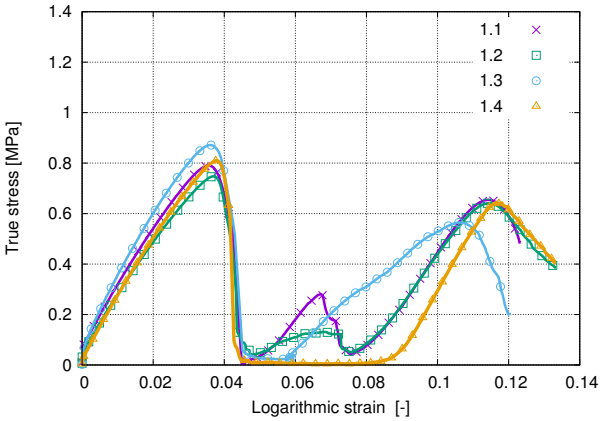

FIGURE 5. Stress-strain curves of specimens in group 1.

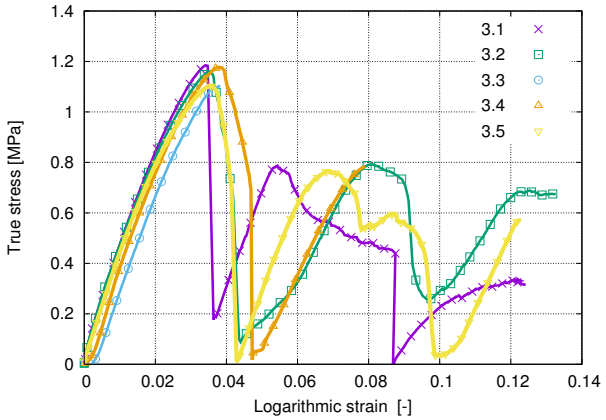

FIGURE 7. Stress-strain curves of specimens in group 3.

3. RESULTS

3.1. STRESS-STRAIN CURVES

A series of uniaxial compressive tests was performed on custom designed three-dimensional inverted honeycomb structures. From the captured loading scenes the evolution of the deformation of the tested structures is assessed. Unfortunately, the base material exhibited a high brittleness which caused failure after the yield strain of the structure. After this failure the loading continued with similar stress-strain behaviour but with a slightly lower stresses at the consequent collapses. True stress vs. logarithmic strain diagrams are depicted in figures 4 to 7 for groups 0 to 3 respectively.

To compare the main mechanical properties of the tested structures and to assess influence of the different reinforcement of the strut joints, mean values among the groups were evaluated with their standard deviations. In table 3 are listed mean ultimate compressive strength (stress at the first collapse), strains corresponding to the first collapse in each group of samples and mean Poisson's ratio in the region up to the first collapse.

4. CONCLUSIONS

An experimental study on deformation response of 3D printed auxetic structures was carried out to evaluate influence of joint properties which were physically simulated by adding an extra amount of material in the struts' connections. The loading setup was equipped with a custom contactless strain measurement system which enabled a precise evaluation of the stress-strain curve. The obtained curves exhibited consistent behaviour among each group (i.e. sphere radius) in terms of stiffness in the linear part, ultimate compressive strength and strain at the first collapse.

The stress level at the first collapse increases with increasing stiffness in the joints, while the strain at the first collapse remains unchanged. The auxetic nature exhibits slight increase when the spheres with the lowest radius are added in the joints' interconnections. Then, with increasing spheres' radius the auxetic behaviour is less significant.
These results show promising possibility of optimisation of the cellular structures based on controlled stiffness in the strut joints. In the further results this knowledge will be employed for optimisation of the auxetics using different materials in the interconnection regions.

Acknowledgements

The financial support of the Czech Science Foundation (project No. 19-23675S).

References

[1] Q. Chen, N. M. Pungo. In-plane elastic buckling of hierarchical honeycomb materials. *European Journal of Mechanics A/Solids* **34**:120–129, 2012. doi:10.1016/j.euromechsol.2011.12.003.

[2] R. Harb, E. Taciroglu, N. Ghoniem. Partitioning of elastic energy in open-cell foams under finite deformations. *Acta Materialia* **61**(5):1454–1468, 2013. doi:10.1016/j.actamat.2012.11.022.

[3] K. A. Dannemann, J. Lankford Jr. High strain rate compression of closed-cell aluminium foams. *Materials Science and Engineering* **293**(1):157–164, 2000. doi:10.1016/S0921-5093(00)01219-3.

[4] R. Lakes. Foam structures with a negative poisson's ratio. *Science* **235**(4797):1038–1040, 1987. doi:10.1126/science.235.4792.1038.

[5] V. S. Deshpande, M. F. Ashby, N. A. Fleck. Foam topology: Bending versus stretching dominated architectures. *Acta materialia* **49**(6):1035–1040, 2001. doi:10.1016/S1359-6454(00)00379-7.

[6] P. Koudelka, O. Jirousek, T. Fila, T. Doktor. Compressive properties of auxetic structures produced by direct 3d printing. *Materiali in Tehnologije* **50**(3):311–317, 2016.

[7] V. Rada, T. Fila, P. Zlamal, et al. Multi-channel control system for in-situ laboratory loading devices. *Acta Polytechnica Proceedings* **18**:15–19, 2018. doi:10.14311/APP.2018.18.0015.

[8] B. D. Lucas, T. Kanade. An iterative image registration technique with an application to stereo vision. *In: Proceedings of Imaging Understanding Workshop* pp. 121–130, 1981.

[9] I. Jandejsek, J. Valach, D. Vavrik. Optimization and calibration of digital image correlation method. *In: Proceedings of Experimental Stress Analysis 2010* pp. 121–126, 2010.

[10] G. Bradski. The opencv library. *Dr Dobb's Journal of Software Tools* 2000. `http://www.drdobbs.com/open-source/the-opencv-library/184404319`.